

Refinable G^1 functions on G^1 free-form surfaces

Kęstutis Karčiauskas^a and Jörg Peters^b
^a Vilnius University ^b University of Florida

Abstract

For two high-quality piecewise polynomial geometrically smooth (G^1) surface constructions, explicit G^1 functions are derived that form the basis of a functions space on the G^1 surfaces. The spaces are refinable and nested, i.e. the functions can be re-represented at a finer level. By choosing all basis functions to be first order smooth a maximal set of degrees of freedom is obtained that have small support and near-uniform layout.

1. Introduction

Subdivision surfaces are defined as a nested sequence of refined representations. This allows for ever finer approximation of their limit and for a natural hierarchy. However, the infinite recursion also complicates the inclusion of subdivision surfaces into existing industrial design infrastructure and postprocessing, such as computing integrals near the extraordinary limit points. Geometrically smooth constructions for filling multi-sided holes, on the other hand, while compatible with existing infrastructure seem to lack refinability, except for trivial splitting by de Casteljau's algorithm. De Casteljau splitting does not provide refined *smooth spaces* with additional degrees of freedom. If the goal is to better match data, alter the design or to animate geometry then re-arranging the initial patch layout can provide the required degrees of freedom. However, when the purpose of the refinable space of compatible G^1 functions [GP15] is to compute on the surface, strict nestedness of the refined spaces is required – if only to apply standard tools and estimates of finite element theory. A standard approach to judge the accuracy of a finite element numerical solution is to compare the solutions before and after nested refinement, and to conclude accuracy within error bounds when the computed function does not change by more than a fraction of the acceptable error. If the refinement is not nested, i.e. if the function space changes at each iteration, then such comparisons can not be made since it is not clear that the sequence with shrinking error converges: the error may shift to different regions with each iteration, increasing the error in some parts of the domain while reducing in others. Moreover, the principles of isogeometric analysis on manifolds [GP15] additionally require that the G^k -construction of the geometry and the analysis functions on the geometry have identical reparameterizations across patch boundaries.

A further reason to investigate nested refinement is that some CAD processes require exact preservation of primary design surfaces when adding detail. Even though

we will not recommend to use all additional degrees of freedom of the refined G-splines *directly* as good handles for modeling, tools could be built to leverage them to support localized adjustments for an otherwise vetted and immutable primary design surface.

While singular parameterization can yield both free-form surfaces and nested, refinable spaces [NP16], this comes at the cost of reduced surface quality. Therefore, this paper exposes the refinability of functions on two recently-developed high-quality G^1 surface constructions: [KP15] of degree bi-5 and [KNP16] of degree bi-4. We illustrate the trade-off between uniformity and locality of refinement for these two algorithms and different choices of smoothness within the refined pieces. To maintain its focus on nested refinability the paper does not present an implementation of applications such as isogeometric analysis on manifolds.

Overview After a brief review of the literature, Section 2 sets the stage for refined multi-sided hole filling and explains the common components of refined constructions: Section 2.1 specializes the G^1 constraints for refining [KP15] and [KNP16], Section 2.2 shows how to preserve curvature continuity at the central point, Section 2.3 shows the generic construction from the surrounding spline complex into the multi-sided surface cap and the refinement away from the geometrically continuous boundaries. Section 3 establishes the properties of the refined functions and Section 4 adds a 2×2 refined biquartic alternative for completeness that may be thought of as just one additional step of refinement. The discussion Section 5 focuses on the choice of degrees of freedom and implementation.

1.1. Literature

Starting with [COS00, CSA⁺02], subdivision functions have repeatedly been used as finite elements, leveraging their natural ability to re-represent functions at a finer, possibly adaptive level to improve solutions. The challenge concerning integration near irregular points was pointed to e.g. in [HKD93, NKP14].

Since matched G^k -constructions always yield C^k -continuous isogeometric elements [GP15], a number of geometrically continuous constructions have been tested for their use in solving higher-order partial differential equations on planar domains, graphs and, without nested refinement, on smooth manifolds. Generalized iso-geometric analysis elements were shown to be effective in [NKP14, KNP16, NKP16]. Geometrically continuous surface constructions, including those of our focus [KP15] and [KNP16], intentionally do not expose all Bézier degrees of freedom that exist after G^1 constraints have been enforced. Rather they harness the asymmetrically-distributed degrees of freedom to optimize shape and provide high-level B-spline-like control points that bake in not only formal smoothness but good shape as verified against a gallery of challenging test cases. However, we do not know how to refine the control net so that the algorithms generate the same surfaces at finer levels.

The present paper takes the approach that the surface (geometry) is determined by the B-spline-like construction that is optimized for good shape – while a set of linearly independent functions provides a maximal set of degrees of freedom for nested refinement of functions on the surface. The goal is to explicitly exhibit these G^1 continuous functions (with the same reparameterizations as the underlying surface), not just count them. This differs both from [MVV16] which, akin to the analysis of C^k functions [LS07], computes the dimension of G^1 spaces for various choices of connectivity and

geometric layout; and from [KVJB15, CST15] that enumerate G^1 transitions between two patches, based on various choices of patch degree, connectivity and geometric layout. This paper sorts the specific degrees of freedom into several classes, depending on their distance to the geometrically continuous patch boundaries.

2. Notation and Geometric continuity

The constructions in [KP15] and [KNP16] focus on a submesh, called *CC-net*, that consists of an irregular node, where $n \neq 4$ quads (4-sided facets or *sectors*) meet, and $6n$ nodes that form two layers of quads surrounding it (the second layer may have irregular nodes). Fig. 1a displays a CC-net plus one additional layer of quads that is not used for the construction of the n -sided *surface cap* but provides, for context, a surface ring (green in Fig. 1b) surrounding the cap. Only the C^2 prolongation of this surface ring towards the center, called a *tensor-border of degree 3 and depth 2* and denoted \mathfrak{t}_3 is needed for the constructions and their refinement.

While the initial geometric constructions [KP15], [KNP16] use, akin to the control points of a tensor-product spline, as degrees of freedom only the nodes of the CC-net, the refined constructions have a variety of different degrees of freedom: bi-cubic B-spline control points, control points of a quadratic expansion at the center and Bézier control points of tensor-product patches. While the additional degrees of freedom were available also for the geometric constructions, they were used to improve shape and simplify the manipulation handles of the surface to mimic a B-spline-net. Now, however, additional degrees of freedom along geometrically reparameterized edges will be exposed – for computing on surfaces rather than for geometric manipulation. This difference is discussed in more detail in Section 5.2.

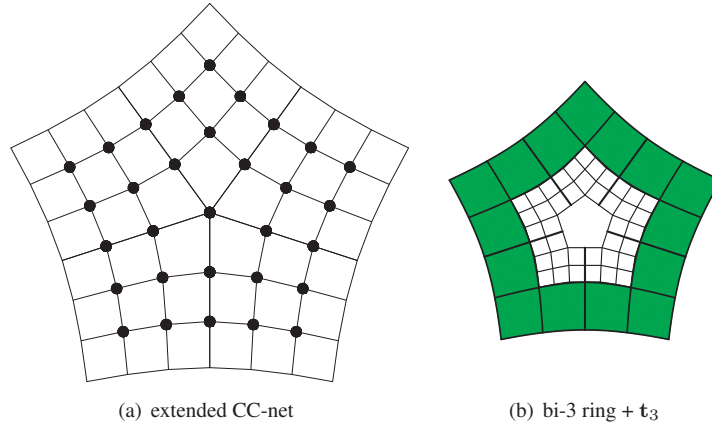


Figure 1: Hole-filling setup from [KP15]. (a) An CC-net extended by one layer for $n = 5$. (b) A regular bi-3 surface layer (green) surrounding a tensor-border \mathfrak{t}_3 of depth 2.

2.1. Geometric continuity under refinement

We construct surface pieces $\hat{\mathbf{p}}$ and $\check{\mathbf{p}}$ mapping $[0..1] \times [0..1] \rightarrow \mathbb{R}^d$ that share a boundary curve $\hat{\mathbf{p}}(u, 0) = \check{\mathbf{p}}(u, 0)$. For geometric constructions typically $d = 3$ and for the refinable function space to be constructed $d = 1$. Moreover, we construct $\hat{\mathbf{p}}$ and $\check{\mathbf{p}}$ so that along their common curve the G^1 constraint holds:

$$\partial_v \hat{\mathbf{p}} - a(u) \partial_v \check{\mathbf{p}} - b(u) \partial_u \check{\mathbf{p}} = 0. \quad (\text{G1})$$

In our refinement constructions $\partial_v \hat{\mathbf{p}}(u, 0)$, $\partial_v \check{\mathbf{p}}(u, 0)$ and $\partial_u \check{\mathbf{p}}(u, 0)$ will be piecewise polynomial functions in u and $a(u)$ and $b(u)$ will be subdivided, hence entire polynomials. Therefore, if $\partial_v \hat{\mathbf{p}}(u, 0)$, $\partial_v \check{\mathbf{p}}(u, 0)$ are C^ν -continuous, the boundary curve $\hat{\mathbf{p}}(u, 0) = \check{\mathbf{p}}(u, 0)$ must be $C^{\nu+1}$ -continuous.

In our constructions there are two types of G -curves of a cap: *sector separating curves* (schematically displayed as the right and the top edges of the subdivided square in Fig. 2(a)) and *input curves* that form the degree 3 border of the cap (left and bottom edge in Fig. 2(a)). Fig. 2(a) also labels, from the center point with index 0 to the corner with index $N = 2^s$, the breakpoints of the $N \times N$ partition of a sector at level s th refinement. The points with indices k and $k + 1$ bound the k th segment.

Structural symmetry, i.e. invariance under reversing the labeling of sectors, across the sector separating curves implies $a(u) := -1$. Both [KP15] and [KNP16] additionally choose $b(u) := 2c(1 - u)$. To match the tensor-border, a second reparameterization is applied across input curves. The reparameterizations will be subdivided along with the surface.

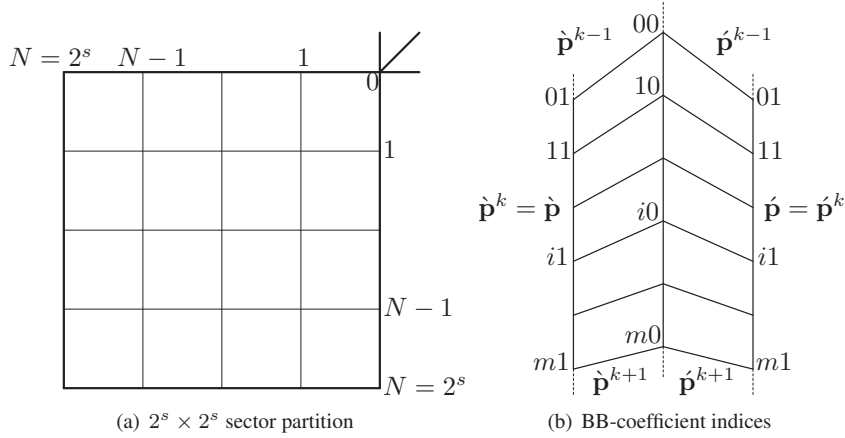


Figure 2: (a) Uniform $2^s \times 2^s$ partition ($s = 2$) of a sector at an irregular point (index 0). The right edge corresponds to sector separating curves defined by $\hat{\mathbf{p}}_{i0}^k$, $k = 0, \dots, 2^{s-1} = N - 1$. The left edge corresponds to the input curve. (b) Indexing symmetric with respect to the sector separating curve for solving (G1).

Denote by \mathbf{p}_{ij} the BB-coefficients of a tensor-product patch \mathbf{p} of bi-degree m de-

defined in terms of the Bernstein-Bézier (BB) polynomials $B_k^m(t)$ of degree m :

$$\mathbf{p}(u, v) := \sum_{i=0}^m \sum_{j=0}^m \mathbf{p}_{ij} B_i^m(u) B_j^m(v), \quad (u, v) \in \square := [0..1]^2.$$

The reparameterization along sector separating curves yields a smooth surface under the following constraints.

Lemma 1 (linear (G1)). *Let $\mathring{\mathbf{p}}, \acute{\mathbf{p}}$ be adjacent patches of degree $bi-m$. For*

$$i = 0, \dots, m, \quad a(u) := -1 \quad \text{and} \quad b(u) := w(1-u) + \bar{w}u,$$

the G^1 constraints (G1) are satisfied if (see Fig. 2(b) for indices)

$$\acute{\mathbf{p}}_{i1} := -\mathring{\mathbf{p}}_{i1} - \frac{i}{m} \bar{w} \mathring{\mathbf{p}}_{i-1,0} + (2 - (1 - \frac{i}{m})w + \frac{i}{m} \bar{w}) \mathring{\mathbf{p}}_{i0} + (1 - \frac{i}{m})w \mathring{\mathbf{p}}_{i+1,0}. \quad (1)$$

In the following it will be convenient to consider the λ th BB-layer of $\mathring{\mathbf{p}}$ consisting of BB-coefficients $\mathring{\mathbf{p}}_{i\lambda}^k$ where $\lambda \in \{0, 1\}$ and $i = 0, \dots, m$ (and analogously for $\acute{\mathbf{p}}$). $\mathring{\mathbf{p}}_{i0}^k$ are coefficients on the k th curve segment shared by two patches $\mathring{\mathbf{p}}$ and $\acute{\mathbf{p}}$. We say that the λ th BB-layer of $\mathring{\mathbf{p}}$ is C^ν -connected if its pieces join C^ν when interpreted as curves, i.e. when $\sum_j \mathring{\mathbf{p}}_{j\lambda}^k B_j^d$ and $\sum_j \mathring{\mathbf{p}}_{j\lambda}^{k+1} B_j^d$ join C^ν for all k .

Noting that subdividing w amounts to choosing $w_{k+1} = \bar{w}_k = \frac{1}{2}(w_k + \bar{w}_{k+1})$, comparing differentiability establishes the following fact.

Proposition 1 (implied smoothness of G^1 refinement). *Assume that two consecutive pairs of subpatches along the sector partition satisfy (1), $\{\mathring{\mathbf{p}}^k, \acute{\mathbf{p}}^k\}$ with (w_k, \bar{w}_k) and $\{\mathring{\mathbf{p}}^{k+1}, \acute{\mathbf{p}}^{k+1}\}$ with (w_{k+1}, \bar{w}_{k+1}) . Let $0 \leq \nu \leq m-1$. Assume that the sector-separating BB-layer $\lambda = 0$ of $\mathring{\mathbf{p}}$ (and hence of $\acute{\mathbf{p}}$) is $C^{\nu+1}$ -connected and BB-layer $\lambda = 1$ of $\mathring{\mathbf{p}}$ is C^ν -connected. If $w_{k+1} = \bar{w}_k = \frac{1}{2}(w_k + \bar{w}_{k+1})$ then the BB-layer $\lambda = 1$ of $\acute{\mathbf{p}}$ is C^ν -connected.*

By setting $a(u) = -1$ and

$$b(u) := w_k(1-u) + \bar{w}_k u, \quad w_k := 2(1 - \frac{k}{N})c, \quad \bar{w}_k := 2(1 - \frac{k+1}{N})c, \quad (2)$$

for the k th segment subpatches of the refined constructions of [KP15] (bi-5) and [KNP16] (bi-4), the assumption $w_{k+1} = \bar{w}_k = \frac{1}{2}(w_k + \bar{w}_{k+1})$ of Proposition 1 holds.

2.2. Curvature continuity at the central point and refinement of quadratic expansion

In the next two sections, we refine near the irregular point and along the input curve – in preparation for refining [KP15] and [KNP16] along sector separating curves. Fig. 3 shows, as green circles, the degrees of freedom of one sector of the tensor-border t_3 , namely bi-cubic B-spline control points. The blue disks in the upper right corner mark the sector's BB-coefficients defined by a unique quadratic at the irregular point. The quadratic provides another six degrees of freedoms.

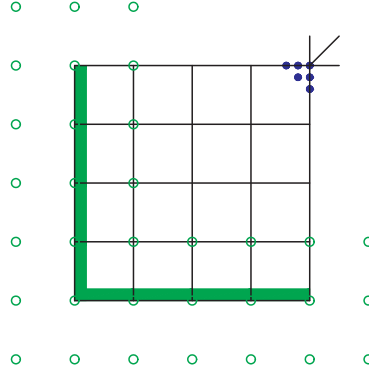


Figure 3: Degrees of freedom along the input curves and BB-coefficients of the quadratic expansion at irregular point.

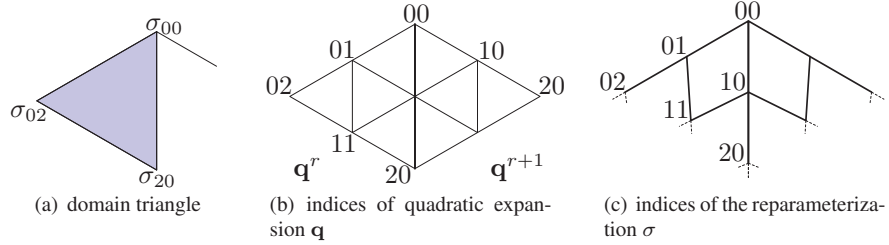


Figure 4: Quadratic expansion and reparameterization at the irregular point.

[KP15] and [KNP16] support high surface quality by curvature continuity at the irregular point. Under refinement we retain curvature continuity at the irregular point as follows. The r th sector of the quadratic expansion is expressed in total degree 2 BB-form with BB-coefficients \mathbf{q}_{ij}^r (see Fig. 4a; the double subscript accounts for rotation from sector to neighboring sector). Taking as free control point:

$$\mathbf{q}_{00}^0, \mathbf{q}_{01}^0, \mathbf{q}_{10}^0, \mathbf{q}_{02}^0, \mathbf{q}_{11}^0, \mathbf{q}_{20}^0, \quad (3)$$

the coefficients of the other sectors are calculated iteratively as

$$\begin{aligned} \mathbf{q}_{00}^{r+1} &:= \mathbf{q}_{00}^r, \quad \mathbf{q}_{01}^{r+1} := \mathbf{q}_{10}^r, \quad \mathbf{q}_{02}^{r+1} := \mathbf{q}_{20}^r, \\ \mathbf{q}_{10}^{r+1} &:= -\mathbf{q}_{01}^r + 2c\mathbf{q}_{10}^r + 2(1-c)\mathbf{q}_{00}^r, \quad \mathbf{q}_{11}^{r+1} := -\mathbf{q}_{11}^r + 2c\mathbf{q}_{20}^r + 2(1-c)\mathbf{q}_{10}^r, \\ \mathbf{q}_{20}^{r+1} &:= \mathbf{q}_{02}^r - 4c\mathbf{q}_{11}^r + 4c^2\mathbf{q}_{20}^r - 4(1-c)\mathbf{q}_{01}^r + 8c(1-c)\mathbf{q}_{10}^r + 4(1-c)^2\mathbf{q}_{00}^r. \end{aligned}$$

Following [KP15] we define a reparameterization σ with BB-coefficients σ_{ij} (Fig. 4b), that is symmetric with respect to rotation and diagonal flip, to satisfy (1) when $k = 0$;

$i = 0, 1$. (Recall that k enumerates the pieces starting at the irregular point).

$$\begin{aligned} \sigma_{00} &:= (0, 0), \quad \sigma_{10} := \frac{1}{2}(\sigma_{00} + \sigma_{20}), \quad \sigma_{11} := \mu \frac{1}{2}(\sigma_{02} + \sigma_{20}) + (1 - \mu)\sigma_{00}, \quad (4) \\ \bar{w} := \bar{w}_0 &:= 2\left(1 - \frac{1}{N}\right)c, \quad \mu := \begin{cases} \frac{10+8c+\bar{w}}{10(1+c)} & \text{for [KP15];} \\ \frac{8+6c+\bar{w}}{8(1+c)} & \text{for [KNP16];} \end{cases} \end{aligned}$$

The coefficients σ_{20} and σ_{02} are set to be the corner points of domain sector triangle of the quadratic expansion \mathbf{q} (see Fig. 4c). Then the second order Hermite expansion of $\mathbf{q} \circ \sigma$ at the origin has the bi-5 [KP15], respectively the bi-4 [KNP16] BB-coefficients

$$\begin{aligned} \mathbf{p}_{00}^r &:= \mathbf{q}_{00}^r, \quad \mathbf{p}_{10}^r := -\mathbf{q}_{00}^r + 2\mathbf{q}_{10}^r, \\ \mathbf{p}_{20}^r &:= \begin{cases} -\frac{1}{2}\mathbf{q}_{00}^r - \mathbf{q}_{10}^r + \frac{5}{2}\mathbf{q}_{20}^r & \text{for [KP15];} \\ -\frac{1}{3}\mathbf{q}_{00}^r - \frac{4}{3}\mathbf{q}_{10}^r + \frac{8}{3}\mathbf{q}_{20}^r & \text{for [KNP16];} \end{cases} \\ \mathbf{p}_{11}^r &:= (-1 - 2\tau)\mathbf{q}_{00}^r + \tau(\mathbf{q}_{10}^r + \mathbf{q}_{01}^r) + 2\mathbf{q}_{11}^r, \\ \tau &:= \begin{cases} \frac{\bar{w}-2c}{5(1+c)} & \text{for [KP15];} \\ \frac{\bar{w}-2c}{4(1+c)} & \text{for [KNP16];} \end{cases} \end{aligned} \quad (5)$$

Symmetric formulas define $\mathbf{p}_{01}^r, \mathbf{p}_{02}^r$. By construction, the \mathbf{p}^r satisfy (1) for $i = 0, 1$.

Since the refinement $(\mathbf{q} \circ \sigma)(u/2, v/2)$ yields the same formula (5) except for N in \bar{w} adjusted to the new refinement level s , we have the following lemma.

Lemma 2 (refinement of central quadratic degrees of freedom). *The six central free control point $\tilde{\mathbf{q}}_{ij}^0$ at level s are obtained from the six \mathbf{q}_{ij}^0 at level $s-1$ as if by de Casteljau's algorithm:*

$$\begin{aligned} \tilde{\mathbf{q}}_{00}^0 &:= \mathbf{q}_{00}^0, \quad \tilde{\mathbf{q}}_{10}^0 := \frac{1}{2}(\mathbf{q}_{00}^0 + \mathbf{q}_{10}^0), \quad \tilde{\mathbf{q}}_{20}^0 := \frac{1}{4}\mathbf{q}_{00}^0 + \frac{1}{2}\mathbf{q}_{10}^0 + \frac{1}{4}\mathbf{q}_{20}^0, \\ \tilde{\mathbf{q}}_{11}^0 &:= \frac{1}{4}(\mathbf{q}_{00}^0 + \mathbf{q}_{10}^0 + \mathbf{q}_{01}^0 + \mathbf{q}_{11}^0). \end{aligned} \quad (6)$$

Symmetry of formulas defines $\tilde{\mathbf{q}}_{01}^0, \tilde{\mathbf{q}}_{02}^0$.

2.3. G^1 refinement along an input curve

Along the input curves, $\mathbf{t}_m = \mathbf{t}_3 \circ \beta$ is of degree m and depth 1 ($m = 5$ in [KP15], $m = 4$ in [KNP16]) with $\mathbf{t}_3 \circ \beta$ the input tensor-border \mathbf{t}_3 reparameterized by

$$\beta := (u + b(u)v, a(u)v) : \quad a(u) := \sum_{i=0}^{m-3} a_i B_i^{m-3}(u), \quad b(u) := \sum_{i=0}^{m-2} b_i B_i^{m-2}(u). \quad (7)$$

Fig. 3 shows as green circles (\circ) the bi-3 B-spline coefficients of the CC-net for a refinement at level $s = 2$. The refinement is based on de Casteljau's algorithm and is summarized in the following lemma.

Lemma 3 (refinement of the tensor-border reparameterization). *Abbreviating the refined tensor-border pieces as*

$$\mathbf{t}_r^{left} := \mathbf{t}_r\left(\frac{u}{2}, \frac{v}{2}\right), \quad \mathbf{t}_r^{right} := \mathbf{t}_r\left(\frac{1}{2} + \frac{u}{2}, \frac{v}{2}\right), \quad r \in \{3, 5\},$$

then $\mathbf{t}_m^{left} = \mathbf{t}_3^{left} \circ \beta^{left}$, $\mathbf{t}_m^{right} = \mathbf{t}_3^{right} \circ \beta^{right}$, where

$$a^{left}(u) := a\left(\frac{u}{2}\right), \quad a^{right}(u) := a\left(\frac{1}{2} + \frac{u}{2}\right), \quad b^{left}(u) := b\left(\frac{u}{2}\right), \quad b^{right}(u) := b\left(\frac{1}{2} + \frac{u}{2}\right).$$

The explicit expressions for the BB-coefficients of a^{left} , a^{right} , b^{left} , b^{right} , starting with the choice of a_i , b_i from [KP15], respectively [KNP16], are

$$\begin{aligned} a_i^{0,0} &:= a_i, \quad i = 0, \dots, m-3, & b_i^{0,0} &:= b_i, \quad i = 0, \dots, m-2, \\ a_i^{s,2k} &:= a_i^{(s-1,k)right}, & b_i^{s,2k} &:= b_i^{(s-1,k)right}, \\ a_i^{s,2k+1} &:= a_i^{(s-1,k)left}, & b_i^{s,2k+1} &:= b_i^{(s-1,k)left}, \end{aligned} \quad (8)$$

where the superscript (s, k) specifies the refinement level s and segment k , $0 \leq k \leq N-1$, $N := 2^s$.

At each intersection \mathbf{p}_{m0}^{N-1} of an input curve and a sector separating curve, the input curve is degree-raised and hence (1) holds for $i = m$. The formulas of Appendix A and

$$\text{[KP15]}: \quad b_3^{s,0} = 0, \quad a_1^{s,0} = \frac{1}{4} a_2^{s,0} (4 - w_{N-1}); \quad (9)$$

$$\text{[KNP16]}: \quad b_2^{s,0} = 0, \quad a_0^{s,0} = \frac{1}{2} a_1^{s,0} (2 - w_{N-1})$$

imply that (1) holds for $i = m-1$. Constraints (9) hold for $s = 0$ with the choice of a_i , b_i of [KP15], [KNP16] and induction confirms that (9) holds under refinement.

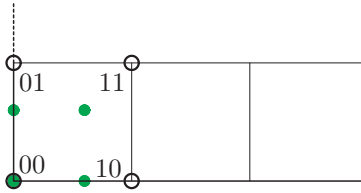


Figure 5: The bi-3 coefficients $\mathbf{t}_{3;ij}^{s,0}$ are shown as black circles, bi-5 coefficients $\mathbf{t}_{5;ij}^{s,0}$ as green disks.

Some care has to be taken for the corner subpatch $\mathbf{p}^{N-1, N-1}$ to be well-defined. The reparameterization must be diagonally symmetric:

$$\mathbf{t}_{m;\bar{i}\bar{j}}^{s, N-1} = \sum_{i=0}^1 \sum_{j=0}^1 e_{ij}^{\bar{i}\bar{j}} \mathbf{t}_{3;ij}^{s, N-1}, \quad e_{ij}^{\bar{i}\bar{j}} = e_{ji}^{\bar{j}\bar{i}} \text{ for } \{\bar{i}, \bar{j}, i, j\} \in \{0, 1\} \quad (10)$$

(see Fig. 5) and (10) holds for

$$a_0^{s,N-1} := 1, b_0^{s,N-1} := 0, a_1^{s,N-1} := \begin{cases} 1 + \frac{3}{2}b_1^{s,N-1}, & \text{[KP15]}, \\ 1 + 2b_1^{s,N-1}, & \text{[KNP16]}. \end{cases} \quad (11)$$

Since (11) holds for the initial

$$\text{[KP15]} : a_0 := 1, a_1 := (1 - \frac{c}{2})a_2; a_2^{def} := 1 + 0.413c + 0.116c^2 \quad (12)$$

$$b_0 = b_2 = b_3 := 0, b_1 := \frac{(2-c)a_2 - 2}{3}$$

$$\text{[KNP16]} : a_0 := 1, a_1 := \frac{1}{1-c}, b_0 = b_2 := 0, b_1 := \frac{c}{2(1-c)}, \quad (13)$$

induction verifies that (11) holds also after refinement.

For the refined tensor-border \mathbf{t}_m , we therefore obtain the following proposition.

Proposition 2 (smoothness along the input curve under refinement). *If $\mathbf{t}_3^{s,k}$ are C^2 -connected and $\mathbf{t}_m^{s,k} := \mathbf{t}_3^{s,k} \circ \beta$ then $\mathbf{t}_m^{s,k-1}$, $\mathbf{t}_m^{s,k}$, $\mathbf{t}_m^{s,k+1}$ are C^1 -connected.*

2.4. G^1 refinement along the sector separating curves

By Proposition 2, the refined sector is only C^1 along the input curve. Therefore, we set the smoothness to be $\nu = 1$. Proposition 1 implies that the sector separating curves are C^2 -connected. Since the layers under consideration all have knots of high multiplicity when expressed in B-spline form, for $m > 3$ it is more convenient to express the *free control points* in BB-form. We recall that two adjacent Bézier curves \mathbf{p} and $\tilde{\mathbf{p}}$ of degree m are C^1 -connected if $\tilde{\mathbf{p}}_0 = \mathbf{p}_m := \frac{1}{2}(\mathbf{p}_{m-1} + \tilde{\mathbf{p}}_1)$ and C^2 -connected if

$$\tilde{\mathbf{p}}_0 = \mathbf{p}_m, \mathbf{p}_{m-1} := \mathbf{p}_m + \frac{1}{4}(\mathbf{p}_{m-2} - \tilde{\mathbf{p}}_2), \tilde{\mathbf{p}}_1 := \mathbf{p}_m - \frac{1}{4}(\mathbf{p}_{m-2} - \tilde{\mathbf{p}}_2).$$

(For C^1 curves, B-spline control points coincide with the ‘inner’ BB-coefficients, for C^2 curves, the B-spline control equals $2\mathbf{p}_{m-1} - \mathbf{p}_{m-2} = 2\tilde{\mathbf{p}}_1 - \tilde{\mathbf{p}}_2$.)

Fig. 6 schematically displays the free control points along the sector separating curve as well as the BB-coefficients derived from the central quadratic and the input tensor-border:

- $\dot{\mathbf{p}}_{i0}^0$, $i = 0, 1, 2$ and $\dot{\mathbf{p}}_{i1}^0$, $i = 0, 1$ are defined by quadratic expansion, see Section 2.2.
- $\dot{\mathbf{p}}_{i0}^{N-1}$ and $\dot{\mathbf{p}}_{i1}^{N-1}$, $i = m-1, m$ are defined by the input bicubic B-spline, see Section 2.3.

For $k = 0, \dots, N-1$, the following BB-coefficients $\dot{\mathbf{p}}_{ij}^k$ can be *independently set* while retaining G^1 continuity (the generic cases for $k = 1, \dots, N-2$ are listed first):

- $\dot{\mathbf{p}}_{i1}^k$, $i = 1, \dots, m-1$, $\dot{\mathbf{p}}_{i1}^0$, $i = 2, \dots, m-1$; $\dot{\mathbf{p}}_{i1}^{N-1}$, $i = 1, \dots, m-2$;

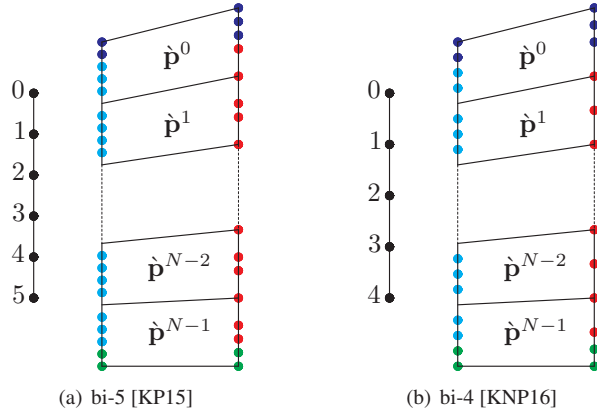


Figure 6: The free control points $\mathbf{g}_\bullet = \mathbf{g}_{i1}^k$ and $\mathbf{g}_\bullet = \mathbf{g}_{i0}^k$ along the sector separating curve, and the points \mathbf{g}_\bullet defined by the tensor-border and \mathbf{g}_\bullet by the central quadratic. The number line to the *left* of each figure shows the indices of the BB-coefficients of the BB-layer curves.

$$\begin{aligned}
 \bullet \text{ [KP15]: } & \dot{\mathbf{p}}_{i0}^k, i = 2, 3, 5; & \dot{\mathbf{p}}_{i0}^0, i = 3, 5; & \dot{\mathbf{p}}_{i0}^{N-1}, i = 2, 3; \\
 \bullet \text{ [KNP16]: } & \dot{\mathbf{p}}_{i0}^k, i = 2, 4, & \dot{\mathbf{p}}_{40}^0; \dot{\mathbf{p}}_{20}^{N-1}.
 \end{aligned}$$

Fig. 7 displays, as black disks, the internal free control point. The gray G^1 strips represent the BB-coefficients of Fig. 6 as defined by Section 2.2, Section 2.3, Section 2.4.

Due to the G^1 constraints, the *refinement rules* for the free control point \mathbf{g}_{ij}^k along the input curve and the central quadratic are best obtained by construction rather than tabulating a large, parameterized family of subdivision stencils.

3. Basis functions and their properties

Setting to 1 the value of one free control point \mathbf{g} and to zero those of all other free control points and then applying the algorithm yields, as a collection of polynomial pieces represented in BB-form, the *G-function* $g_{\mathbf{g}}$ of \mathbf{g} . For simplicity, we denote, along the sector separating curve, as g_{ij}^k the G-function for the control point \mathbf{g}_{ij}^k . Although the value of \mathbf{g}_{ij}^k coincides with that of $\dot{\mathbf{p}}_{ij}^k$ used in the previous section, we assign different symbols to make clear that the function associated with \mathbf{g}_{ij}^k is a piecewise polynomial G-function, whereas the function associated with $\dot{\mathbf{p}}_{ij}^k$ is a Bernstein polynomial.

3.1. Support and BB-coefficients of G-functions

Since interior G-functions are tensor-product B-splines, their support is well-known. Near sector boundaries the additional knot line limits their support to the sector. Similarly, the B-splines along the input curve and corresponding to the regular part, with free control points g_\bullet (see Fig. 3), are well-understood. Fig. 8(c) shows only their support inside the cap at the intersection of the input boundary and the sector separating curve. Fig. 8(d,e) display the generic supports along the sector separating curve. At the ends, the support does not exceed the sector boundaries. For $m = 5$, we list, as

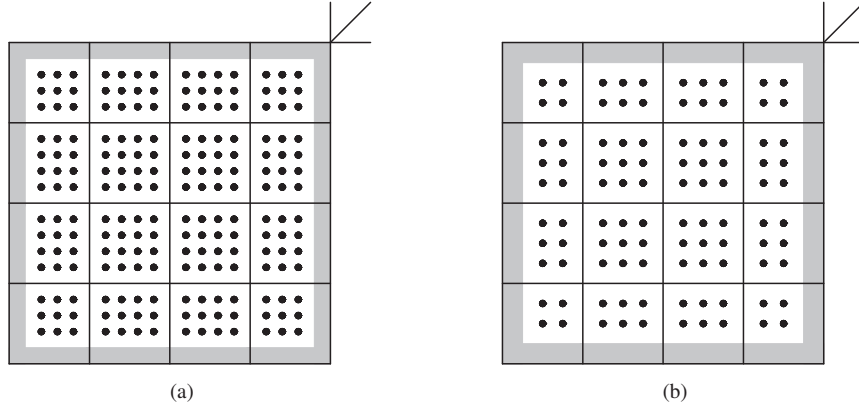


Figure 7: free control points of internal C^1 refinement: (a) bi-5 [KP15]; (b) bi-4 [KNP16].

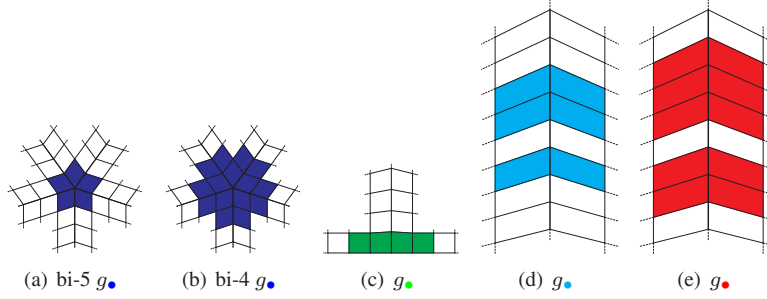


Figure 8: Supports of basis functions g : (a,b) quadratic expansions for $m = 4, 5$. (c) intersection of input curve and sector separating curve, (d) first BB-layer (generic case) *top* four quads: for indices $i = 1, m - 1$, *bottom* two quads for $i = 2, m - 2$; bi-4: *top* for indices $i = 1, 3$, *bottom* for $i = 2$, (e) sector separating curve (generic case) *top* six quads: for $i = 2$ and $m = 4$, *bottom* four quads for $i = 4$.

explicit examples, the BB-coefficients of some G-functions. Noting that $\hat{\mathbf{p}}_{5\lambda}^k = \hat{\mathbf{p}}_{0\lambda}^{k+1}$ and that $\hat{\mathbf{p}}_{j_0}^k = \hat{\mathbf{p}}_{j_0}^k$ is the sector separating curve, we only list nonzero rows. The bold 1 marks the BB-coefficient of the G-function g_{ij}^k that is obtained, as we recall, by

setting $\mathbf{g}_{ij}^k = 1$ and all other free control points to zero.

$$\begin{array}{c}
 \left[\begin{array}{ccc}
 \dot{\mathbf{p}}_{01}^k & \dot{\mathbf{p}}_{00}^k & \dot{\mathbf{p}}_{01}^k \\
 11 & 10 & 11 \\
 21 & 20 & 21 \\
 31 & 30 & 31 \\
 41 & 40 & 41 \\
 \dot{\mathbf{p}}_{51}^k & \dot{\mathbf{p}}_{50}^k & \dot{\mathbf{p}}_{51}^k \\
 11 & 10 & 11 \\
 21 & 20 & 21 \\
 31 & 30 & 31 \\
 41 & 40 & 41 \\
 \dot{\mathbf{p}}_{51}^{k+1} & \dot{\mathbf{p}}_{50}^{k+1} & \dot{\mathbf{p}}_{51}^{k+1}
 \end{array} \right] \\
 \text{along sector separating curve} \\
 \underbrace{\left[\begin{array}{ccc}
 1 & 0 & -1 \\
 \frac{1}{2} & 0 & -\frac{1}{2}
 \end{array} \right]}_{\bullet g_{41}^k} \quad
 \underbrace{\left[\begin{array}{ccc}
 1 & 0 & -1
 \end{array} \right]}_{\bullet g_{31}^k} \quad
 \underbrace{\left[\begin{array}{ccc}
 0 & 0 & \frac{2w_k}{5} \\
 0 & 1 & \frac{2+4w_{k+1}}{5} \\
 0 & 1 & 2 \\
 0 & 1 & \frac{2-4w_{k+1}}{5} \\
 0 & 0 & -\frac{2w_{k+2}}{5}
 \end{array} \right]}_{\bullet g_{50}^k}
 \end{array} \tag{14}$$

Leveraging symmetry and shift, there are relatively few different patterns for the BB-coefficients of G-functions to store.

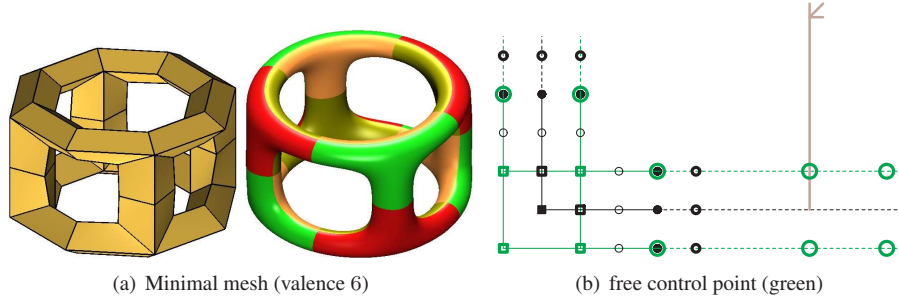


Figure 9: Directly adjacent caps. (b) The green circles represent B-spline control points of the first BB-layer curve and the green squares are BB-coefficients on the curve.

Proposition 3 (Linear Independence). For each of [KP15] and [KNP16], for each level of refinement, the G-functions $g_{\mathbf{g}}$ associated with the free control points \mathbf{g} form a basis of a corresponding space of G^1 functions.

Proof The linear independence of the G-functions $g_{\mathbf{g}}$ associated with the free control points \mathbf{g} follows from four observations (color coded as in the previous bullet list).

- \mathbf{g}_o The bi-3 B-splines of the tensor-border are linearly independent over the regular region outside the cap. When caps abut directly there is no regular region. Then the thick hollow markers in Fig. 9(b) (green circles for B-spline control points and green squares for BB-coefficients) represent the free control points of the first BB-layer curves to either side of the input curve. (The first BB-layer curves determine the input curve via C^1 constraints.)

- g. The interior G-functions are C^1 B-splines of degree bi- m , hence linearly independent.
- g. The quadratic at the irregular point is defined by the six free control points of (3). The corresponding six G-functions are linearly independent.
- g.,g. The corresponding G-functions along the sector separating curve are linearly independent since, by construction, only g_{ij}^k has a non-zero BB-coefficient $\dot{\mathbf{p}}_{ij}^k$.

No non-zero BB-coefficient of g. or g. is an independently-set BB-coefficient $\dot{\mathbf{p}}_{ij}^k$ along the sector separating curve (cf. Section 2.4), and the interior G-functions g. do not share non-zero BB-coefficients with any other type of G-function. Therefore the four types of G-functions together are linearly independent. $\quad |||$

4. G^1 refinement of 2×2 bi-4 surfaces

Although valences $n = 3, 4, 5, 6$ often suffice for design of free-form surfaces for completeness, we discuss the structurally similar refinement of 2×2 bi-4 patches per sector from [KNP16] intended for caps with higher valences such as Fig. 10(a). For implementation, we may treat the resulting functions as one level more refined than the ‘unsplit’ bi-4 construction.

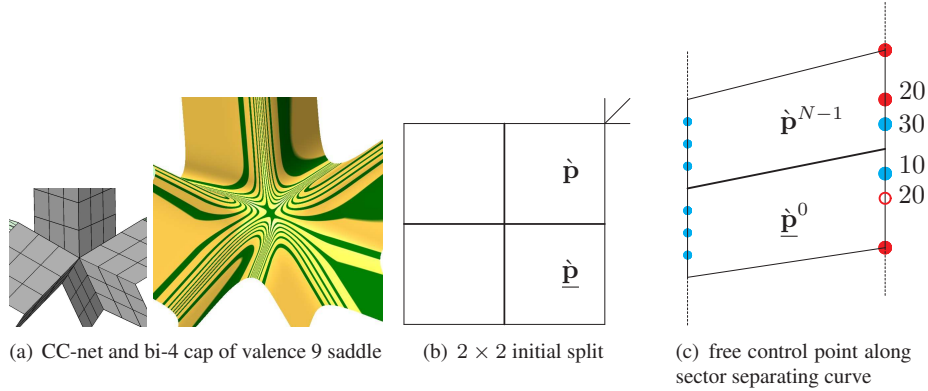


Figure 10: Initial 2×2 partition and free control point.

According to [KNP16]

$$\begin{aligned} \text{top: } (\dot{\mathbf{p}}) \quad a(u) &:= -1, \quad b(u) := w(1-u) + \bar{w}u; \\ \text{bottom: } (\dot{\mathbf{p}}) \quad \underline{a}(u) &:= -1, \quad \underline{b}(u) := \underline{w}(1-u) + \underline{\bar{w}}u, \end{aligned} \quad (15)$$

where $\underline{w} = \underline{\bar{w}} = \gamma$, $w := 2c$, $\bar{w} = 0$, $\gamma^{def} := 1.13 - 0.9c + 0.36c^2$. Since (1) applies separately to the top and the bottom patches, the refinement of w , \bar{w} and $\dot{\mathbf{p}}_{i1}^{N-1}$, $\dot{\mathbf{p}}_{i0}^0$ (small cyan free control point) are those of the unsplit construction and we choose $\nu = 1$. However, since $\bar{w} \neq \frac{1}{2}(w + \underline{\bar{w}})$, the sector separating curve is only C^1 across

the split (cf. Fig. 10b) yielding additional free control point $\dot{\mathbf{p}}_{30}^{N-1}$ and $\dot{\mathbf{p}}_{10}^0$ (big cyan disks). The top and bottom pieces of the cap are C^1 -connected by setting

$$\begin{aligned}\dot{\mathbf{p}}_{40}^{N-1} = \dot{\mathbf{p}}_{00}^0 &:= \frac{1}{2}(\dot{\mathbf{p}}_{30}^{N-1} + \dot{\mathbf{p}}_{10}^0). \\ \dot{\mathbf{p}}_{20}^0 &:= \dot{\mathbf{p}}_{20}^{N-1} + \frac{14\bar{w}^{N-1} - w^{N-1} - \bar{w}^0}{6\bar{w}^{N-1}}(\dot{\mathbf{p}}_{10}^0 - \dot{\mathbf{p}}_{30}^{N-1}).\end{aligned}$$

- The quadratic expansion is refined according to the unsplit bi-4 construction except that initially $\bar{w} := \gamma^{def} \neq 0$.
- The tensor-border is refined according to the unsplit bi-4 construction, except that (13) is replaced by the more general choice

$$a_0 := 1, \quad a_1 := \frac{1}{1 - \gamma c}, \quad b_0 = b_2 := 0, \quad b_1 := \frac{\gamma c}{2(1 - \gamma c)}.$$

We note that since $b(u)$ and $\underline{b}(u)$ join only with continuity, the remark following (G1) on $C^{\nu+1}$ continuity of the sector separating curve therefore does not apply. Analogously to Proposition 3, we can prove that the G-functions $g_{\mathbf{g}}$ associated with the free control points \mathbf{g} form a basis of a corresponding space of G^1 functions.

5. Discussion

Balancing the number of special cases of refinable basis functions against their support size is an important choice when refining. Smaller support offers finer resolution that, while undesirable in the context of high-quality surface constructions, can reduce the number of refinement steps and yield more localized interaction of derivatives in the finite element context. Moreover, increased internal smoothness to reduce the growth of degrees of freedom can complicate implementation. We illustrate this trade-off between uniformity and locality below.

5.1. Refinable functions with higher internal continuity

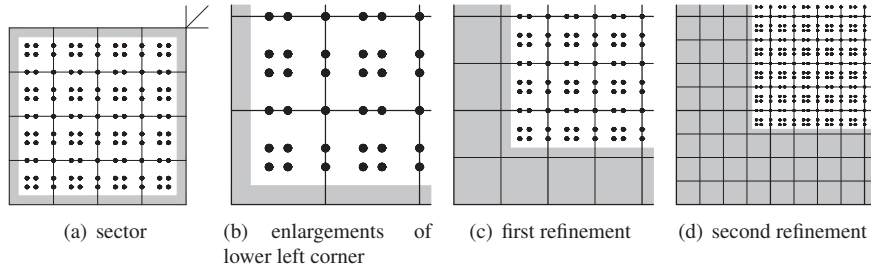


Figure 11: Mixture of internal C^1 and C^2 continuity. The gray strips are neighborhoods of refined G^1 curves (boundary and sector separating curves). Disks mark free control point of the internal C^2 connected patches.

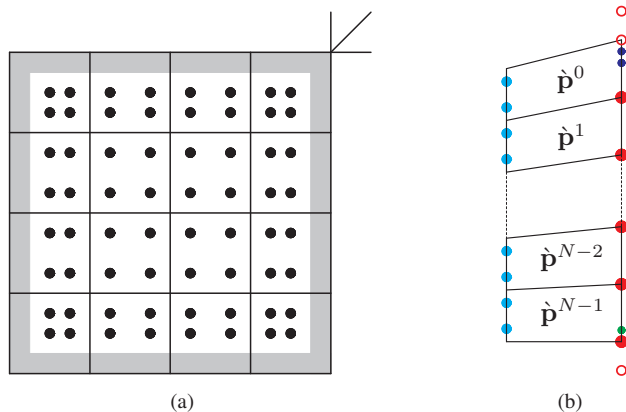


Figure 12: (a) The free control points of internally C^3 bi-5 sector. (b) C^3 -connected cyan and C^4 -connected red BB-layers.

Since the initial caps of [KP15] and [KNP16] are formally only G^1 (although prolonging second order Hermite data), it seems unnecessary to increase internal smoothness of the sectors beyond C^1 . Moreover increasing internal continuity complicates implementation: with each refinement (cf. Fig. 11b,c,d) more BB-layers of patches across the input curves inherit C^1 continuity.

The growth of C^1 BB-layers, which is caused by the refinement of C^1 -reparameterized input data, can be avoided by adaptively refining only near the irregular point and not along the input curve. For [KP15] bi-5 the internal continuity can then be $\nu \leq 3$ (by Observation 1, the sector separating curve is C^4 for $\nu = 3$; see Fig. 12), while for [KNP16] bi-4, $\nu \leq 2$ since a C^4 quartic is global and yields no additional free control point via refinement.

5.2. The computational rather than geometric role of the additional free control point

Fig. 13 shows raised a part of the sector separating curve at refinement level $s = 2$ of [KP15]. The closeup Fig. 13d shows that raising just the g_\bullet free control point along the sector separating curve yields an asymmetric BB-net (as expected from (14)). Only if both g_\bullet and g_\circ are used together is the new feature aligned with the sector separating curve, Fig. 13e. We explain the nature of the asymmetry by reference to the curve case. Consider a ($u = \text{const}$) parameter-curve perpendicular to the sector separating curve. We simplify matters by stipulating that the two degree 3 curve segments \mathbf{b}^0 and \mathbf{b}^1 (with BB-coefficients $\mathbf{b}_j^k, j \in \{0, 1, 2, 3\}$) join C^1 at $\mathbf{b}_0^k = \mathbf{b}_3^{k-1} = (\mathbf{b}_2^{k-1} + \mathbf{b}_1^k)/2$, as in Fig. 14. The inner BB-coefficients $\mathbf{b}_1^k, \mathbf{b}_2^k$ a co-located with the double-knot B-spline coefficients (black disks in the top polygon of Fig. 14a). The endpoints \mathbf{b}_0^k and \mathbf{b}_3^k (circles) are their averages due to the C^1 join and Fig. 14a shows the corresponding two-piece spline curve in the *middle*. Alternatively, the same spline curve is defined by a less symmetric set of control points \mathbf{b}_2^k (cyan) and \mathbf{b}_3^k (red disks) (Fig. 14a *bottom*). These control points also determine the remaining \mathbf{b}_1^k (marked as circles) by the C^1 constraints. However, manipulating the top control polygon by pulling up the B-spline

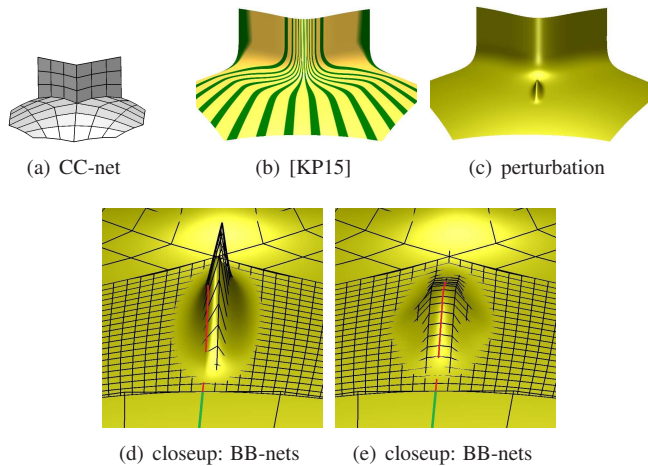


Figure 13: (a) input $n = 6$ CC-net and (b) bi-5 [KP15] surface; (c,d) naive direct manipulation with free control point; (e) modification via auxiliary 'height' function.

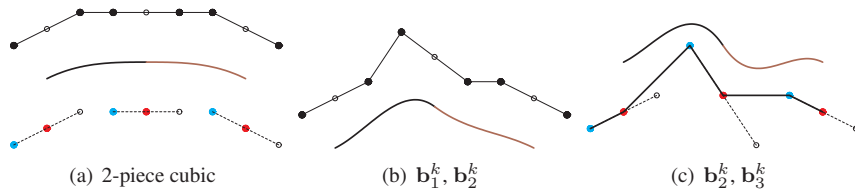


Figure 14: Univariate analogue explaining the geometric effects of different choices of free control point (cf. Fig. 13).

control point \mathbf{b}_2^0 (black disk, Fig. 14b) changes the curve gently while applying the same change to \mathbf{b}_2^k (cyan disk in Fig. 14c) for the bottom choice of free control point, results in a large oscillation and thus mimics perturbing g_\bullet and g_\circ). We conclude that the additional free control point obtained by refinement along the sector separating curve are not for direct surface manipulation.

5.3. Implementation

Compared to generalized subdivision algorithms, such as Catmull-Clark subdivision [CC78], the implementation needs to keep track of the refinement level s and location $k \in [0, 1, \dots, N - 1, N := 2^s]$ with respect to the initial G^1 patch boundaries. However, in terms of s and k there are relatively few special G^1 refinement patterns, essentially of those of type (6), (14) and Appendix A.

6. Conclusion

By subdividing the reparameterization along the initial geometric G^1 patch boundaries, we were able to explicitly generate a maximal set of G^1 functions that refine the

space of the initial high-quality geometric construction in a nested hierarchy. There are four types of basis functions, each with localized support. Such a space can be used, for example, to compute elastic shell properties for a given free-form geometry.

Acknowledgements The work was supported in part by NSF Grant CCF-1117695.

- [CC78] E. Catmull and J. Clark. Recursively generated B-spline surfaces on arbitrary topological meshes. *Computer-Aided Design*, 10:350–355, September 1978.
- [COS00] F. Cirak, M. Ortiz, and P. Schröder. Subdivision surfaces: A new paradigm for thin-shell finite-element analysis. *Internat. J. Numer. Methods Engrg.*, 47(12):2039–2072, 2000.
- [CSA⁺02] F. Cirak, M.J. Scott, E. K. Antonsson, M. Ortiz, and P. Schröder. Integrated modeling, finite-element analysis, and engineering design for thin-shell structures using subdivision. *Computer-Aided Design*, 34(2):137–148, 2002.
- [CST15] Annabelle Collin, Giancarlo Sangalli, and Thomas Takacs. Approximation properties of multi-patch C^1 isogeometric spaces. *arXiv:1509.07619*, 2015.
- [GP15] David Groisser and Jörg Peters. Matched G^k -constructions always yield C^k -continuous isogeometric elements. *Computer Aided Geometric Design*, 34:67–72, 2015.
- [HKD93] Mark Halstead, Michael Kass, and Tony DeRose. Efficient, fair interpolation using Catmull-Clark surfaces. In *Proceedings of the 20th Annual Conference on Computer Graphics and Interactive Techniques*, SIGGRAPH '93, pages 35–44, New York, NY, USA, 1993. ACM.
- [KNP16] Kęstutis Karčiauskas, Thien Nguyen, and Jörg Peters. Generalizing bicubic splines for modelling and IGA with irregular layout. *Computer Aided Design*, 70:23–35, Jan 2016.
- [KP15] Kęstutis Karčiauskas and Jörg Peters. Improved shape for multi-surface blends. *Graphical Models*, 8:87–98, 2 2015.
- [KVJB15] M. Kapl, V. Vitrih, B. Jüttler, and K. Birner. Isogeometric analysis with geometrically continuous functions on two-patch geometries. *Comp and Math with Appl*, 70(7):1518–1538, 2015.
- [LS07] Ming-Jun Lai and Larry L. Schumaker. *Spline Functions on Triangulations*. Encyclopedia of Mathematics and its Applications. 2007.
- [MVV16] Bernard Mourrain, Raimundas Vidunas, and Nelly Villamizar. Dimension and bases for geometrically continuous splines on surfaces of arbitrary topology. *Computer Aided Geometric Design*, 45:108–133, 2016.

- [NKP14] Thien Nguyen, Kęstutis Karčiauskas, and Jörg Peters. A comparative study of several classical, discrete differential and isogeometric methods for solving poisson's equation on the disk. *Axioms*, 3(2):280–299, 2014.
- [NKP16] Thien Nguyen, Kęstutis Karčiauskas, and Jörg Peters. C^1 finite elements on non-tensor-product 2d and 3d manifolds. *Applied Mathematics and Computation*, online:148–158, to appear 2016.
- [NP16] Thien Nguyen and Jörg Peters. Refinable C^1 spline elements for irregular quad layout. *Computer Aided Geometric Design*, pages 123–130, March 29 2016.

Appendix A

Along the input curve, the BB-coefficients $\mathbf{t}_{m;i0}$, $i = 0, \dots, m$, ($m = 4, 5$) are obtained from $\mathbf{t}_{3;i0}$, $i = 0, \dots, 3$, by degree-raising. For the first interior layer

$$\begin{aligned} \mathbf{t}_{4;1} &:= \frac{1}{16}A_{4;0}\mathbf{t}_{3;0} + \frac{1}{16}A_{4;1}\mathbf{t}_{3;1}; \quad \mathbf{t}_{5;1} := \frac{1}{50}A_{5;0}\mathbf{t}_{3;0} + \frac{1}{50}A_{5;1}\mathbf{t}_{3;1}, \\ \mathbf{t}_{3;0} &:= (\mathbf{t}_{3;00}, \dots, \mathbf{t}_{3;30})^t, \quad \mathbf{t}_{3;1} := (\mathbf{t}_{3;01}, \dots, \mathbf{t}_{3;31})^t, \\ \mathbf{t}_{4;1} &:= (\mathbf{t}_{4;01}, \dots, \mathbf{t}_{4;41})^t, \quad \mathbf{t}_{5;1} := (\mathbf{t}_{5;01}, \dots, \mathbf{t}_{5;51})^t \end{aligned}$$

$$A_{4;0} := \begin{pmatrix} 16-12(a_0+b_0) & 12b_0 & 0 & 0 \\ 4-3(a_1+2b_1) & 12-3(3a_0+2b_0-2b_1) & 6b_0 & 0 \\ -2b_2 & 8-2(3a_1+4b_1-b_2) & 8-2(3a_0+b_0-4b_1) & 2b_0 \\ 0 & -6b_2 & 12-3(3a_1+2b_1-2b_2) & 4-3(a_0-2b_1) \\ 0 & 0 & -12b_2 & 16-12(a_1-b_2) \end{pmatrix},$$

$$A_{5;0} := \begin{pmatrix} 50-30(a_0+b_0) & 30b_0 & 0 & 0 \\ 20-6(2a_1+3b_1) & 30-6(3a_0+2b_0-3b_1) & 12b_0 & 0 \\ 5-3(a_2+3b_2) & 30-9(2a_1+2b_1-b_2) & 15-3(3a_0+b_0-6b_1) & 3b_0 \\ -3b_3 & 15-3(3a_2-b_3+6b_2) & 30-9(2a_1+b_1-2b_2) & 5-3(a_0-3b_1) \\ 0 & -12b_3 & 30-6(3a_2-2b_3+3b_2) & 20-6(2a_1-3b_2) \\ 0 & 0 & -30b_3 & 50-30(a_2-b_3) \end{pmatrix},$$

$$A_{4;1} := \begin{pmatrix} 12a_0 & 0 & 0 & 0 \\ 3a_1 & 9a_0 & 0 & 0 \\ 0 & 6a_1 & 6a_0 & 0 \\ 0 & 0 & 9a_1 & 3a_0 \\ 0 & 0 & 0 & 12a_1 \end{pmatrix}, \quad A_{5;1} := \begin{pmatrix} 30a_0 & 0 & 0 & 0 \\ 12a_1 & 18a_0 & 0 & 0 \\ 3a_2 & 18a_1 & 9a_0 & 0 \\ 0 & 9a_2 & 18a_1 & 3a_0 \\ 0 & 0 & 18a_2 & 12a_1 \\ 0 & 0 & 0 & 30a_2 \end{pmatrix}.$$